NANO LETTERS

2008
Vol. 8, No. 8
2253-2257

Capillary Absorption of Metal Nanodroplets by Single-Wall Carbon Nanotubes

D. Schebarchov[†] and S. C. Hendy[*,†,‡]

School of Chemical and Physical Sciences, Victoria University of Wellington, Wellington 6001, New Zealand, and MacDiarmid Institute for Advanced Materials and Nanotechnology, Industrial Research Ltd, Lower Hutt 6009, New Zealand

Received March 27, 2008; Revised Manuscript Received May 15, 2008

ABSTRACT

We present a simple model that demonstrates the possibility of capillary absorption of nonwetting liquid nanoparticles by carbon nanotubes (CNTs) assisted by the action of the Laplace pressure due to the droplet surface tension. We test this model with molecular dynamics simulation and find excellent agreement with the theory, which shows that for a given nanotube radius there is a critical size below which a metal droplet will be absorbed. The model also explains recent observations of capillary absorption of nonwetting Cu nanodroplets by carbon nanotubes. This finding has implications for our understanding of the growth of CNTs from metal catalyst particles and suggests new methods for fabricating composite metal−CNT materials.

Soon after the discovery of carbon nanotubes (CNTs),[1] it was suggested that their thermal, electronic, mechanical, and optical properties could be enhanced by combining them with other materials. On the basis of computer simulations, it was predicted that open CNTs might act as "molecular straws" capable of absorbing dipolar molecules by capillary action.[2] Since then, a number of methods have been developed to fill CNTs,[3] and the novel properties associated with the composite nanofibers have found applications in electronics, catalysis, separation, and storage technology.[3–7] In addition, CNTs filled with nanoparticles have been used to form devices such as high-frequency oscillators[8] and nanopipettes.[9]

It was also suggested that CNTs could be used as molds for encapsulating metal nanowires.[4] Encapsulating a metal wire inside a CNT would protect it from oxidation and prevent breakup by Rayleigh and Peierls instabilities,[10] for instance. However, further studies by Dujardin et al.[11,12] led to the conclusion that only low surface tension melts ($\gamma <$ 100−200 mN m^{-1}) could be drawn into the inner cavity of nanotubes through capillary action. Since most pure metals do not wet graphite ($\theta_c > 90°$), it was deduced that capillary action alone is not sufficient to fill CNTs with pure metals.

However, this deduction was based on the equations for bulk capillarity, and it is not clear whether the argument extends to the nanoscale. Indeed, there is certainly experimental evidence that nanoparticles can be drawn easily into open CNTs. For instance, nanoparticles of various transition metals such as Pd, Ni, and Cu, which are used as catalysts during the growth of CNTs via chemical vapor deposition (CVD) techniques,[13] are often found encapsulated in CNTs during and after the CVD process.[14–17] In addition, Hayashi et al. have recently synthesized vertically aligned CNTs filled with segmented Pd−Co nanocomposites,[18] and Zhang et al. report the filling of CNTs by nonwetting Cu nanodroplets.[19] These experimental observations suggest that capillary forces may be sufficient to drive filling of CNTs by metallic nanoparticles despite the failure of these metals to wet graphite.

In this Letter we present a simple model which suggests that sufficiently small liquid metal droplets can, in fact, be drawn inside a CNT via capillary action. The theory associated with penetration of a small droplet into a capillary has previously been studied by Marmur,[20,21] who was the first to observe that capillary absorption of a droplet could occur even at contact angles higher than 90° provided the droplet was small enough. Our model goes beyond Marmur's work and considers capillary absorption of droplets that are supported by a flat substrate. We then test this model with molecular dynamics (MD) simulations of palladium nanodroplets and find excellent agreement between theory and simulation as to the critical size below which uptake occurs. These results could have important implications for the fabrication of composite nanowires and could also improve our understanding of the relationship between the size of

[†] School of Chemical and Physical Sciences, Victoria University of Wellington.

[‡] MacDiarmid Institute for Advanced Materials and Nanotechnology, Industrial Research Ltd.

10.1021/nl080875s CCC: $40.75 © 2008 American Chemical Society
Published on Web 07/03/2008

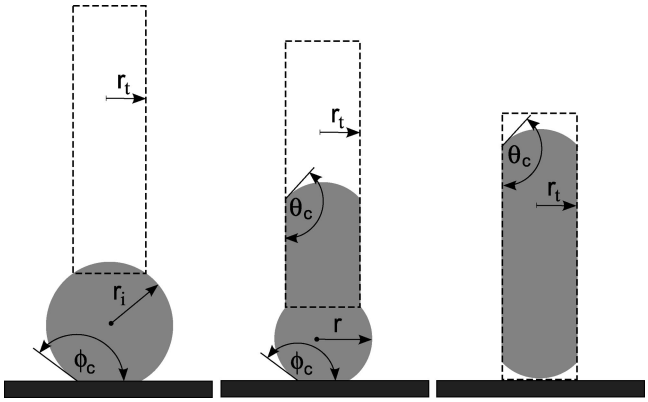

Figure 1. These are the three geometries compared in our model: supported droplet near the tube's opening (left), droplet partially drawn inside the tube (middle), and the fully encapsulated particle (right). Five independent parameters are used to describe these geometries: r_t, r_i, r, ϕ_c, and θ_c. The tube's inner cavity has a circular cross section of radius r_t. The initial shape of the supported droplet is approximated with a spherical cap of radius r_i and a contact angle ϕ_c. During encapsulation, the protruding droplet diminishes in size and the cylindrical column rises inside the capillary tube. The meniscus profile is approximated with a spherical cap forming a contact angle θ_c with the inside wall.

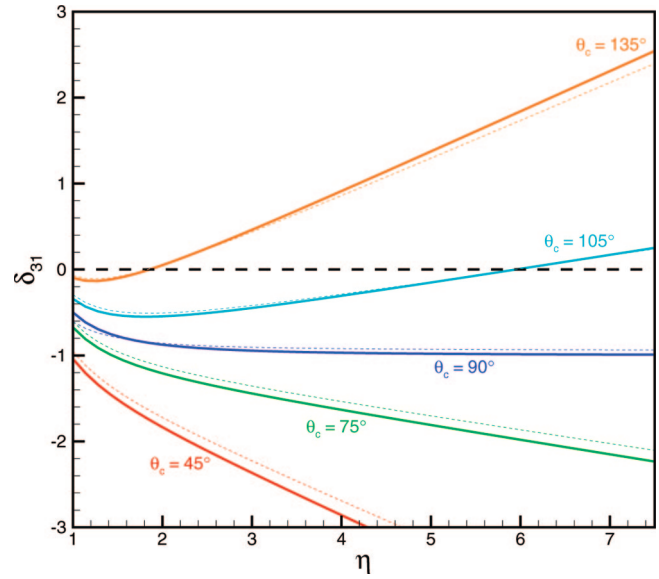

Figure 2. Even if $\theta_c > 90°$, δ_{31} can be negative for sufficiently small η. This implies that droplets of nonwetting melts will prefer encapsulation provided their initial radius of curvature is small enough. The solid curves were plotted for the unsupported case ($\phi_c = 180°$), while the thin dashed lines correspond to $\phi_c = 135°$.

catalyst particles and the diameters of carbon nanotubes that grow from them.[22]

Macroscopically, the sign and magnitude of the pressure difference ΔP across the liquid meniscus depend on the contact angle θ_c

$$\Delta P = \frac{2\gamma \cos \theta_c}{r} \tag{1}$$

where γ is the surface tension of the liquid and r is the radius of curvature of the meniscus. If $\theta_c < 90°$, ΔP is positive, resulting in spontaneous absorption of the liquid into the capillary tube. On the other hand, liquids with $\theta_c > 90°$ will not be drawn inside the hollow unless external forces are applied. However, if a small droplet is present near the opening of the tube, the capillary force will depend not only on the pressure difference across the meniscus but also on the Laplace pressure acting on the surface of the protruding droplet. As we discuss below, our model accounts for this additional force and predicts that the finite size of the particle will allow capillary absorption of nonwetting melts.

In our model we simply compare the total surface free energies of the three scenarios depicted in Figure 1: a spherical droplet near the opening of a tube; a droplet of the same volume partially absorbed inside the tube; and a droplet of the same volume fully encapsulated inside the tube. We thus neglect the effects of line tension and gravity and assume that the density remains constant upon encapsulation. The surface energy associated with each interface is expressed as the product of the surface area (A_i) with the corresponding interfacial energy (γ_i). The surface energies per unit area of the droplet, the tube, and the substrate are γ_d, γ_t, and γ_s, respectively. The quantities γ_{dt} and γ_{ds} represent the interfacial energies per unit area associated with the droplet−tube and droplet−substrate interfaces. The contact angles ϕ_c and θ_c are then obtained from the Young equation; that is, $\gamma_d \cos \phi_c = \gamma_s - \gamma_{ds}$ and $\gamma_d \cos \theta_c = \gamma_t - \gamma_{dt}$.

After expressing the total surface energy associated with each geometry (Γ_1, Γ_2, and Γ_3), assuming that the surface energies are not altered by the curvature or chirality of the tube, we define the energy differences: $\Delta\Gamma_{21} \equiv \Gamma_2 - \Gamma_1$ and $\Delta\Gamma_{31} \equiv \Gamma_3 - \Gamma_1$. Dividing through by $4\pi r_i^2 \gamma_d$, we can eliminate the surface energies using the Young equation, yielding two dimensionless functions, namely, $\delta_{21}(\theta_c, \phi_c, \eta, \xi)$ and $\delta_{31}(\theta_c, \phi_c, \eta)$, which depend on four dimensionless parameters: θ_c, ϕ_c, $\eta \equiv r_i/r_t$ and $\xi \equiv r/r_t$. Note that these parameters are bounded: θ_c and ϕ_c lie between 0 and π, and $1 < \xi < \eta$. The physical interpretation of these functions is straightforward: whenever $\delta_{31} < 0$, the nanoparticle prefers complete encapsulation to no encapsulation; if $\delta_{21} < 0$, the nanoparticle prefers to be partially drawn inside the tube rather than no encapsulation.

The function δ_{31} can be written as a polynomial in η, whose coefficients depend on θ_c and ϕ_c

$$\delta_{31}(\theta_c, \varphi_c, \eta) = \frac{A_{31}(\theta_c)}{\eta^2} + B_{31}(\theta_c, \varphi_c)\eta + C_{31}(\varphi_c) \tag{2}$$

where

$$A_{31} = \frac{1}{3}\left(\frac{1}{1+\sin\theta_c} + \sin\theta_c\right)$$

$$B_{31} = -\frac{1}{6}\cos\theta_c(2+\cos\varphi_c)(1-\cos\varphi_c)^2$$

$$C_{31} = -\frac{1}{6}(2+\cos\varphi_c)(1-\cos\varphi_c)^2$$

It is easy to show algebraically that δ_{31} is always negative if $\theta_c < 90°$, implying that partially wetting droplets will always prefer encapsulation regardless of their size. The plot of δ_{31} versus η is displayed in Figure 2, and it clearly shows that sufficiently small droplets will still prefer encapsulation even for $\theta_c > 90°$. One can equate (2) to zero and solve the

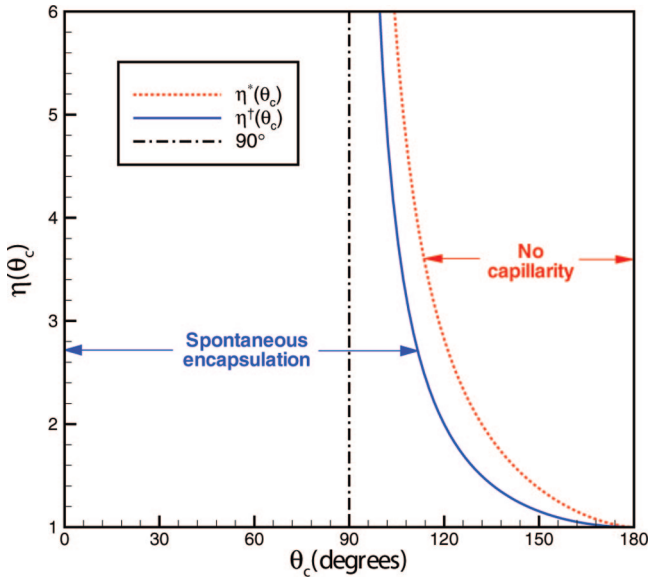

Figure 3. Three capillarity regimes for unsupported droplets. The area to the left of the solid curve ($\eta^{\dagger}(\theta_c)$) corresponds to spontaneous capillary absorption. The area to the right of the dotted curve ($\eta^{*}(\theta_c)$) corresponds to no capillarity. The narrow gap between the two curves is the region of activated capillarity. Note that the region of spontaneous encapsulation extends beyond the macroscopic boundary ($\theta_c = 90°$).

resultant cubic for η, yielding the maximum value of η for which the spherical droplet will prefer full encapsulation for a given contact angle. For $\theta_c < 90°$, there are no physical solutions to eq 2 (i.e., encapsulation preferred at all sizes), while for $\theta_c > 90°$ there is just one physical solution $\eta^{*}(\theta_c) > 1$ (plotted in Figure 3 for the case when $\phi_c = 180°$). However, even if encapsulation is preferred, the supported droplet near the tube's opening will have to go through the intermediate geometry of partial encapsulation. The relative energetics associated with this set of intermediate configurations can be written as

$$\delta_{21}(\theta_c, \varphi_c, \eta, \xi) = \frac{A_{21}(\theta_c, \varphi_c, \xi)}{\eta^2} + B_{21}(\theta_c, \varphi_c)\eta + C_{21}(\varphi_c) \quad (3)$$

and the three coefficients are

$$A_{21} = \frac{1}{6}\left[\frac{1}{1+\sin\theta_c} + \sin\theta_c + \cos\theta_c\sqrt{\xi^2-1}\right] + \frac{\xi}{12}(2\xi\cos\theta_c + 3)[\xi\cos\varphi_c(\cos^2\varphi_c - 3) + 2\sqrt{\xi^2-1}]$$

$$B_{21} = -\frac{1}{6}\cos\theta_c(2+\cos\varphi_c)(1-\cos\varphi_c)^2$$

$$C_{21} = -\frac{1}{6}(2+\cos\varphi_c)(1-\cos\varphi_c)^2$$

As before, we have three parameters (θ_c, ϕ_c, and η) plus another free parameter ξ, which is the dimensionless radius of curvature of the protruding droplet. Extremising (3) with respect to ξ yields the only real stationary point: $\xi^{\dagger} = -1/\cos\theta_c$, and it is a local maximum in the physically plausible region. This local maximum represents an energy barrier that must be overcome to achieve capillary absorption. The value of $\xi^{\dagger}$ is positive only for $\theta_c > 90°$, which means it becomes physically meaningful only in the nonwetting case. However, it is also necessary to satisfy the geometric requirement that $1 < \xi < \eta$. Hence, by equating $\xi^{\dagger} = \eta^{\dagger}$, we can define

$$\eta^{\dagger} = -\frac{1}{\cos\theta_c} \quad (4)$$

which yields the critical particle radius below which the spherical droplet will experience no energy barrier while entering the hollow of the tube. We note that in the limit of an unsupported particle (i.e., $\phi_c \rightarrow 180°$), this expression for $\eta^{\dagger}$ becomes equivalent to that derived by Marmur.[20]

As expected, our model predicts that liquid droplets exhibiting at least partial wetting ($\theta_c < 90°$) of the tube will undergo spontaneous capillary action and fill the tube, regardless of droplet size. This is consistent with the macroscopic theory of capillarity. However, according to the model, even if $\theta_c > 90°$, the droplet will still be absorbed provided it satisfies $\eta < \eta^{\dagger}$. Nonwetting droplets in the region $\eta^{\dagger} < \eta < \eta^{*}$ will prefer encapsulation, but an energy barrier will oppose their entry into the hollow of the tube. We refer to this particular region as activated capillarity. Nonwetting clusters with $\eta > \eta^{*}$ will find it energetically favorable to remain outside the capillary tube. The three different capillarity regimes for unsupported droplets are depicted in Figure 3. We note that the contact angle of CNT-encapsulated Cu nanoparticles recently observed in ref 19 was estimated to be between 120 and 135°. For CNTs of internal radius 20 nm, this corresponds to a critical droplet radius for Cu encapsulation between 30 and 40 nm.

A simple physical explanation for why nonwetting droplets may undergo spontaneous capillary action lies in the consideration of the Laplace pressure acting on the protruding spherical cap. This extra force acts toward the tube and drives the droplet inside the hollow, even if the pressure associated with the meniscus at the other end opposes capillary action. The effect of the Laplace pressure will be diminished if the droplet is supported on a substrate, but it will be present nonetheless provided the interaction between the substrate and the droplet is relatively weak. Increasing the droplet−substrate contact angle ϕ_c will diminish the maximum droplet volume that will be drawn inside the capillary for a given θ_c.

We now test these predictions for the case when $\phi_c = 180°$ (i.e., when the droplet is unsupported) using MD simulation. In the simulations we used a zigzag (38,0) single-wall CNT 220 Å long and 30 Å in diameter, with all carbon atoms fixed in space. Note that the ends of the tube were carbon terminated as might be expected during nanotube growth. Although the choice of termination may affect the energy barrier for encapsulation, we would not expect the final equilibrium state of the droplet to depend on this, except perhaps in the limit of very small droplets or tubes. The droplet used was a molten palladium cluster with a radius of 23 ± 1 Å, and all Pd atoms were modeled with a generalized embedded-atom method (EAM) potential.[23,24] The C−Pd interaction was approximated by a Lennard-Jones (6-12) potential with $\sigma = 2.926$ Å, as in ref 25 and the ε parameter was adjusted to produce the desired contact angle. Note that it is possible that the wetting angle of the droplet may depend on the chirality of the tube, but this is an effect that is neglected in our model above. The time step was set

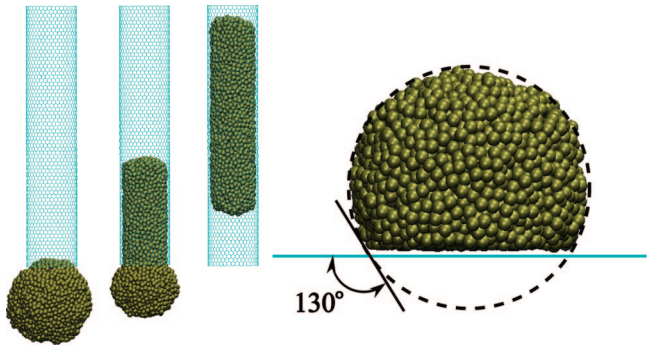

Figure 4. (left) Snapshots of the molten Pd particle (46 Å in diameter) being absorbed by a 30 Å diameter single-wall CNT for $\varepsilon = 31.8$ meV. (right) Snapshot of the molten Pd particle on a graphene sheet. For this value of ε the contact angle formed by the droplet on a flat sheet of graphene is very close to 130°. Note that the meniscus formed by the encapsulated droplet is clearly convex.

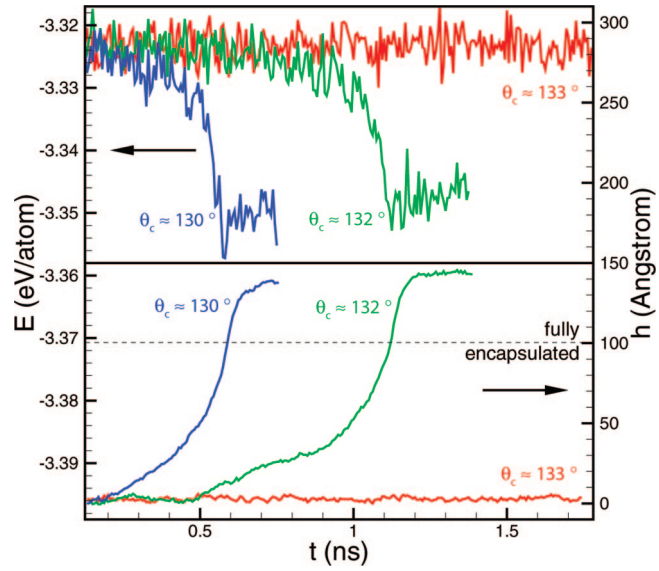

Figure 5. Dynamics of the capillary absorption for three different contact angles. The top panel traces the time evolution of the potential energy, E, while the bottom panel plots the meniscus height h vs time. For contact angles of 130° and 132°, the meniscus rises superlinearly with time and coincides with a drop in the potential energy as the droplet is absorbed.

to 2.5 fs, ensuring adequate conservation of energy during the simulations which were carried out without the use of a thermostat.

Initially, the Pd particle was equilibrated in the absence of a CNT or substrate for 0.25 ns reaching a temperature of approximately 1730 K, and its average radius $\langle R \rangle$ was calculated during a further 0.25 ns. To estimate the contact angle, the molten Pd droplet was deposited on a fixed graphene sheet and equilibrated for a number of ε values. By assuming the droplet had a geometry close to that of a spherical cap (see Figure 4; in the regime of interest here the cap geometry appears to be a good approximation to the droplet shape), we calculated θ_c by measuring the average height $\langle h \rangle$ of the cap during the simulation. With this approach, θ_c was found to vary linearly with ε in the region $40° < \theta_c < 150°$, which provided us with reasonably accurate control over the wetting angle.

The equilibrated spherical droplet of $\langle R \rangle \approx 23$ Å was then placed adjacent to the open end of the fixed CNT with diameter of 30 Å. This particular geometry yields $\eta \approx 1.5$, and our model predicts spontaneous capillary absorption for $\theta_c < 130°$ with a region of activated capillary absorption $130° < \theta_c < 145°$. Figure 4 illustrates the simulated capillary absorption of a nonwetting molten Pd droplet that was found to form a contact angle of $130 \pm 1°$ on graphene. Note that the encapsulated particle clearly displays a convex meniscus inside the CNT. During absorption we find that the meniscus and droplet temperature rise superlinearly, while the droplet potential energy decreases as shown in Figure 5. In this simulation the temperature increased by ~180 K during absorption. This particular simulation result verifies our model's prediction that nonwetting melts can be drawn inside a tube via capillary action.

However, our model also predicts that given $\eta \approx 1.5$, droplets with $\theta_c > 130°$ should experience an energy barrier opposing their entry into the hollow of the tube. To put this to the test, more simulations were carried out with this geometry, but with smaller values of ε. Figure 5 displays the time evolution of meniscus height inside the CNT, as well as the potential energy associated with the Pd particle, for a number of contact angles. Molten nanoparticles with $\theta_c \leq 130°$ were drawn almost immediately. The simulation with $\theta_c \approx 132°$ exhibited a slightly delayed capillary absorption as well as fluctuations of the meniscus velocity. These observations are consistent with the presence of a small energy barrier, which suggests that at 132° the absorption is activated. Our simulations did not yield capillary absorption of the droplets for $\theta_c \geq 133°$.

In conclusion, we have presented a model that predicts capillary absorption of nonwetting molten nanoparticles by CNTs below a critical droplet size. This result has been found to be consistent with molecular dynamics simulations, indicating that it extends to the nanoscale and provides an explanation for recent experimental observations of the absorption of nonwetting Cu nanodroplets by CNTs. The results here also suggest an upper limit on the diameter of a CNT that can be grown from a catalyst particle of a given size. If the catalyst particle is too small relative to the size of the nucleated tube, the particle will presumably be absorbed during growth which may then terminate. Such a limit appears to be consistent with observations of the relationship between tube diameter and catalyst particle size.[22] Thus we expect that this result will have interesting implications for our understanding of the growth of CNTs and may lead to new synthetic routes for composite nanofibers as well as production of nanodevices from CNTs and metal nanoparticles.

References

(1) Iijima, S. *Nature* **1991**, *354*, 56.
(2) Pederson, M. R.; Broughton, J. Q. *Phys. Rev. Lett.* **1992**, *69*, 2689.
(3) Banhart, F.; Grobert, N.; Terrones, M.; Charlier, J. C.; Ajayan, P. M. *Int. J. Mod. Phys. B* **2001**, *15*, 4037.
(4) Ajayan, P. M.; Iijima, S. *Nature* **1993**, *361*, 333.
(5) Tsang, S. C.; Harris, P. J. F.; Green, M. L. H. *Nature* **1993**, *362*, 520.

(6) Tsang, S. C.; Chen, Y. K.; Harris, P. J. F.; Green, M. L. H. *Nature* **1994**, *372*, 159.
(7) Che, G.; Lakshmi, B.; Martin, C.; Fisher, E. *Langmuir* **1999**, *15*, 750.
(8) Gibson, R. F.; Ayorinde, E. O.; Wen, Y. F. *Compos. Sci. Technol.* **2007**, *67*, 1.
(9) Hwang, H. J.; Byun, K. R.; Kang, J. W. *Physica E* **2004**, *23*, 208.
(10) Urban, D. F.; Grabert, H. *Phys. Rev. Lett.* **2003**, *91*, 256803.
(11) Dujardin, E.; Ebbesen, T. W.; Hiura, H.; Tanigaki, K. *Science* **1994**, *265*, 1850.
(12) Dujardin, E.; Ebbesen, T. W.; Krishnan, A.; Treacy, M. M. J. *Adv. Mater.* **1998**, *10*, 1472.
(13) Terranova, M.; Sessa, V.; Rossi, M. *Chem. Vap. Deposition* **2006**, *12*, 315.
(14) Chan, L. H.; Hong, K. H.; Lai, S. H.; Liu, X. W.; Shih, H. C. *Thin Solid Films* **2003**, *423*, 27.
(15) Zhang, G. Y.; Wang, E. G. *Appl. Phys. Lett.* **2003**, *82*, 1926.
(16) Hayashi, Y.; Tokunaga, T.; Toh, S.; Moon, W. J.; Kaneko, K. *Diamond Relat. Mater.* **2005**, *14*, 790.
(17) Ajayan, P. M.; Colliex, C.; Lambert, J. M.; Bernier, P.; Barbedette, L.; Tence, M.; Stephan, O. *Phys. Rev. Lett.* **1994**, *72*, 1722.
(18) Fujita, T.; Hayashi, Y.; Tokunaga, T.; Butler, T.; Rupesinghe, N. L.; Teo, K. B. K.; Amaratunga, G. A. J. *Appl. Phys. Lett.* **2007**, *90*, 133116.
(19) Zhang, Q.; Qian, W. Z.; Yu, H.; Wei, F.; Wen, Q. *Appl. Phys. A: Mater. Sci. Process.* **2007**, *86*, 265.
(20) Marmur, A. *J. Colloid Interface Sci.* **1988**, *122*, 209.
(21) Marmur, A. *Adv. Colloid Interface Sci.* **1992**, *39*, 13.
(22) Nasibulin, A. G.; Pikhitsa, P. V.; Jiang, H.; Kauppinen, E. I. *Carbon* **2005**, *43*, 2251.
(23) Johnson, R. A. *Phys. Rev. B* **1989**, *39*, 12554.
(24) Zhou, X. W.; Johnson, R. A.; Wadley, H. N. G. *Phys. Rev. B* **2004**, *69*, 144113.
(25) Sankaranarayanan, S. K. R. S.; Bhethanabotla, V. R.; Joseph, B. *Phys. Rev. B* **2005**, *72*, 195405.

NL080875S